Laminin–Dynamic Bonds Enable Multifunctionality in a Biological 2D Network

Thanga Bhuvanesh, Yan Nie, Rainhard Machatschek,* Nan Ma,* and Andreas Lendlein

A layer of laminins, assembled on a thin sheet of collagen type IV (Col-IV) forms the backbone of the basal lamina, which controls biological processes such as embryogenesis, tissue homeostasis, and development. Here, the dynamic functions of laminin-111 (Lam-111) in ultrathin films at the air–water interface are investigated. It is shown that the 2D confinement induces polymerization and that expansion via adlayer formation occurs only with extended growth time. The highly robust self-assembly enables the functionalization of surfaces with cross-linked 2D Lam-111 networks of defined thickness using little more than a beaker. The 2D laminin material also displays two dynamic functions required for the maintenance of tissues – the capability for self-renewal and self-healing. By assembling Lam-111 2D networks at the surface of Col-IV sheets, freestanding bilayers closely mimicking the basal lamina can be produced in vitro. There is a marked difference in miPSC spreading and adhesion force between Lam-111 sheets assembled in the presence or absence of Col-IV. These fundamental studies highlight the importance of dynamic functions, encoded into the molecular structure of the building blocks, for the assembly, maintenance, and functioning of the complex material systems found in natural tissues and can provide cues for the molecular design of resilient technical systems.

T. Bhuvanesh, Y. Nie, R. Machatschek, N. Ma, A. Lendlein
Institute of Active Polymers
Helmholtz-Zentrum Hereon
Kantstrasse 55, 14513 Teltow, Germany
E-mail: rainhard.machatschek@hereon.de; nan.ma@hereon.de
T. Bhuvanesh, A. Lendlein
Institute of Chemistry
University of Potsdam
Karl-Liebknecht-Str. 24/25, 14476 Potsdam, Germany
Y. Nie, A. Lendlein
Institute of Biochemistry and Biology
University of Potsdam
Karl-Liebknecht-Str. 24/25, 14476 Potsdam, Germany
N. Ma, A. Lendlein
Institute of Chemistry and Biochemistry
Freie Universität Berlin
14195 Berlin, Germany

1. Introduction

2D materials are commonly defined as inorganic or organic sheets composed of covalently connected atoms or molecules, often arranged on a periodic lattice.[1,2] Graphene and its structural analogs are the most widely recognized 2D materials because of their distinct mechanical, electrical, optical, or magnetic properties.[3] Other 2D materials based on organic molecules arranged with long-range order also have potential applications such as gas separation membranes, chemical recognition sensors, and in electronic or optical devices.[1] However, major challenges hinder their widespread application. The synthesis of large-area, cohesive 2D materials is still an unresolved challenge, especially for crystalline materials, where lateral sizes are determined by the nucleation density. In addition, tailoring the functional properties of 2D materials is complicated by a number of prerequisites toward their constituents regarding valence, size ratio, binding strength, etc., which need to be fulfilled to produce sheet-like materials.

In contrast to their synthetic counterparts, all 2D materials found in nature are amorphous, yet still highly multifunctional. A prominent example is the lipid bilayer forming the cell membrane, which is a very dynamic, quasi-2D material capable of fulfilling a variety of distinct roles using different functionalities.[4] It consists of a variety of different components that enable multifunctionality through their individual molecular features, combined in a defined spatial arrangement. While cells influence the construction of their cellular envelope via the sequence in which they produce and secrete the building blocks, they are clearly not able to control their spatial arrangement in a top-down manner. Rather, the building blocks are inserted via specific and directional interactions with their designated neighbors. In that way, the composition and organization of the cellular membrane are programmed into its molecular building units. Here, the cell's capabilities for the production of nanoscopic structures are far ahead of today's state-of-the-art synthetic methods, which can achieve the bottom-up assembly of nanoscopic structures like dots, rods, or platelets, but not control the distribution of different functional units within these structures.[5]

Another quasi-2D material of paramount importance in nature is the basal lamina (BL), which is essential for biological
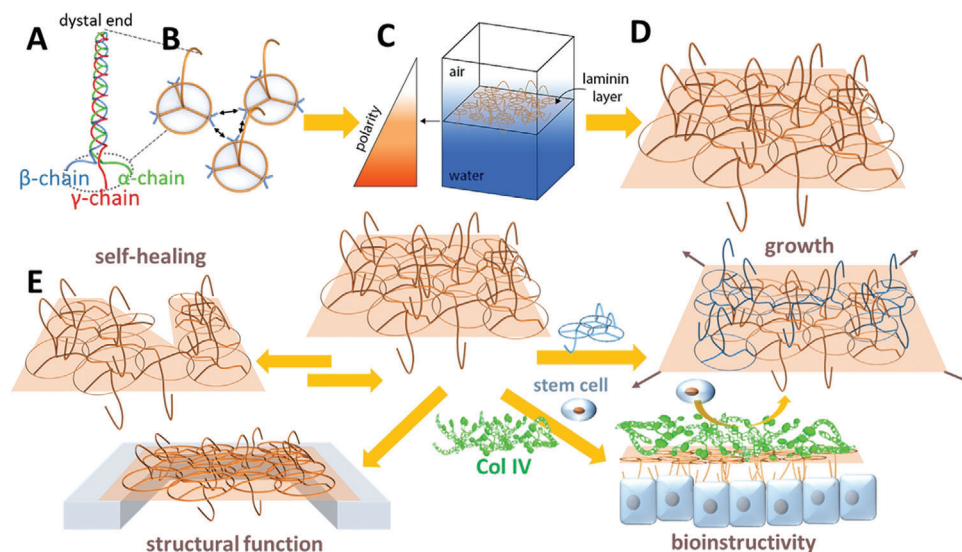
Figure 1. A) Structure of laminin molecules consisting of a triple-helical long arm splayed into three short arms at one distal end. B) Laminin polymerization via ternary interactions of the LN-domains C) Polarity gradient-driven assembly of laminin 2D sheets at the A–W interface D) Schematic representation of laminin 2D network. E) Functions of the laminin 2D network, either by itself or in combination with collagen IV as found in the basal lamina.

processes such as embryogenesis, cell polarization, and tissue homeostasis. As the outer layer of the epithelium, the BL carries out a variety of other important biological functions. It acts as a selective chemical barrier controlling the exchange of substances between different tissue compartments[6] and as a physical barrier between the epithelium and the underlying connective tissue.[7] Models suggest that it consists of two molecular layers: One layer of collagen type IV (Col IV) and one layer of laminins, where the laminins are in direct contact with the basal surface of the epithelial cells.[8] The layer of laminin provides binding sites for adhesion receptors such as integrins at the cell surface, while the layer of Col IV serves as a scaffold that ensures structural stability in the face of mechanical stimuli.[9] The BL is a dynamic network that can change its chemical and physical properties through protein synthesis/degradation or reorganization, resulting in changes in its features, such as thickness and mechanical properties.[10] Those alterations in the BL can, for example, be related to developmental processes and diseases.

Naturally, the BL also incorporates the basic functions required for the maintenance and health of all tissues, such as the capability to grow, self-repair small mechanical damage, and perpetually self-renew to compensate for continuous chemical damage. In consequence, multiple functions are molecularly encoded into the laminins, namely bioinstructivity, self-renewal, self-repair, structural functions, and the capability to grow.

Laminins have a cross-shaped structure (**Figure 1**A), with the long arm of the cross ($\approx$72 nm in length) composed of an α-helical coiled-coil from three chains (α, β, and γ), whereas the three short arms (β, γ chains: 34 nm and α chain: 50 nm in length) are composed of one chain each with an LN domain at the distal end (Figure 1A).[11] Sixteen laminin isoforms have been identified depending on the combination of various α, β, and γ chain subunits.[12] The globular LG – domains at the end of

the long arm bind to cellular receptors, including integrins, α-dystroglycan, heparan sulfates, and sulfated glycolipids.[11] The elevated local concentration of laminins after secretion into the space between the epithelial cells and the Col IV membrane promotes self-assembly through non-covalent α-β-γ ternary interactions of the LN domains.[11,13] The Lam-111 ($\alpha1\beta1\gamma1$) subtype is part of the embryonic epithelium and brain blood vessels. It is the most investigated isoform, as it can be obtained easily in large amounts from a tumor mouse model.[14] It supports the survival, proliferation, and differentiation of many cell types including induced pluripotent stem cells (iPS), Schwann cells, and neural cells through the engagement of integrin proteins such as $\alpha6\beta1$, $\alpha3\beta1$, $\alpha7\beta1$, and $\alpha6\beta4$.[12,15]

While it is not completely understood how they arrange in the BL, their valence of three and their assembly via ternary interactions make laminins ideal building blocks for natural 2D materials (Figure 1C).[16] Their multivalent nature ensures that a tightly connected network is formed even when not every molecule uses all of its binding sites. The reversible formation of the non-covalent bonds is key to enabling the dynamic functions of the networks such as self-healing and growth (Figure 1D), while the organization of the BL is encoded into the laminins via molecular recognition of highly selective interacting domains. The three binding sites define a single binding plane which promotes the formation of 2D structures, but since the molecules are flexible and can probably also rotate around the binding sites, as with most 2D materials, synthesis under 2D confinement is essential to ensure that the material becomes 2D.[17] Commonly, it is assumed that this 2D confinement in nature is achieved via anchorage of the laminins to the cellular membrane via their long arm.[8] This would also result in an alignment of the molecules in a way that all long arms are on the same side of the laminin network, creating a 2D network with two distinct faces. Alternatively, the confinement could also be a consequence of the very

2304268 (2 of 13)

limited space between the epithelial cells and the Col IV layer of the basal lamina.

As a result and in contrast to phospholipids, assembling laminins into 2D networks as found in nature, thereby activating all the functions encoded into their molecular structure, remains an unresolved challenge. Here, we hypothesize that the air–water (A–W) interface can be used to prepare and characterize such highly multifunctional laminin 2D networks and to create BL-like 2D sheets of Col IV and laminins (Figure 1F). This approach takes advantage of the amphiphilic character of laminins, in particular, Lam-111. The high concentration of molecules in the monolayer induces the polymerization of the 2D network. Similar to the growth of the laminin layers in vivo, which is supported by the secretion of laminins by the cells into the extracellular fluid, the aqueous subphase acts as a reservoir for laminin molecules that can be integrated into the 2D network to enable both growth and renewal. Using the Langmuir technique, the adsorption of the laminins at the interface can be easily followed using surface pressure measurements and ellipsometry, allowing to determine the influence of pH and ionic strength on the kinetics of Lam-111 adsorption. By means of interfacial rheology, the self-crosslinking of the laminin monolayer can also be quantified. In situ polarization modulation-infrared reflection absorption spectroscopy (PM-IRRAS) can determine the conformation of the molecules in the networks and, to a certain degree, their orientation. Here, an important question is whether the polarity gradient between air and water is sufficient to orient the molecules in a way that the long arms are on a distinct side of the 2D network, as realized in nature. A parallel orientation with respect to the A–W interface might be energetically favored if the long arm has no inherent polarity gradient, resulting in an equal distribution of long arms on both sides of the 2D sheet. In that case, the assembly of Lam-111 at a preformed Col IV layer could promote a preferential orientation via molecular recognition.[18] A preferential orientation of the cell-adhesive domains on the long arms could direct the cell attachment toward a distinct face of the BL. Enabling different cellular adhesion forces on the two distinct faces of the BL introduces the potential for bioinstructivity, which may be vital to cell polarization. Here, this is quantified by measuring the adhesion forces between induced pluripotent stem cells from mice (miP-SCs) and Lam-111 / Col IV bilayer materials, which are carried out after transfers to solid substrates while selectively generating different bilayer orientations. The adhesion force measurements are complemented by assessing single cell miPSC adhesion and spreading after 48 h. The single-cell passaging approach is currently being explored to address the limitations of colony passaging.[19] However, single-cell passaging still presents significant challenges, including compromised cell survival and poor cloning efficiency. Lam-111, which is present in early embryos, promotes the proliferation of miPSC via integrin-dependent signaling pathways. Substrates with optimal Lam-111 presentation could therefore support single-cell passaging, with miPSC acting as sensitive probes for the presentation of the Lam-111 cell-binding domains. The 2D self-cross linking of laminins imparts remarkable mechanical stability, enabling the BL to provide mechanical support to the epithelial cells. Here, we show that the BL-mimicking Col IV-laminin bilayers are freestanding on porous surfaces. But also, the Lam-111 2D networks can form freestanding structures on their own, that can be transferred onto TEM-

grids covered with a lacey carbon film (Figure 1E). Transferred films are also used to show the nanostructured network organization of the 2D network by Atomic Force Microscopy (AFM). The self-healing capability of Lam-111 2D networks is conveniently quantified in situ using interfacial rheology. To investigate the growth of Lam-111 layers and the self-renewal through the dynamic exchange of molecules, rhodamine-labeled Lam-111 (LamRho) is injected into the subphase under pre-formed Lam-111 layers. By transfer after 4 and 10 h, the inclusion of the new molecules can be visualized via fluorescence.

The extremely robust self-assembly encoded into laminins facilitates the formation of 2D networks using little more than a beaker and a syringe while their strong cohesion suggests that multilayers can be prepared with high control over the deposited amount, shown here for up to 5 layers using AFM and PM-IRRAS. The simple and reliable protocol for producing Lam-111 layers with defined thickness introduced here will be of great value for studies relying on laminin coatings for cell adhesion.

2. Results and Discussion

2.1. Self-Assembly and Self-Cross-Linking

At the A–W interface, Lam-111 assembles in a monolayer where self-crosslinking is promoted by the high areal concentration. After spreading the molecules from the aqueous solution, Brewster angle microscopy indicated a smooth layer, homogenous on the microscale, where an increase in reflectivity with time was clearly apparent (Figure S1, Supporting Information). An important prerequisite to achieve a high surface excess during spreading is to ensure that sufficient molecules can adsorb at the A–W interface, which was achieved by simulating the acidic nature of sulfated glycolipids on cell membranes using a subphase with acidic pH, which promoted anchorage of Lam-111 at the interface. Further, the ions Na^+, Cl^-, and Ca^{2+} present in the extracellular space of cells ($[Na^+] \approx 140$ mm; $[Cl^-] \approx 100$ mm; $[Ca^{2+}] \approx 1.8$ mm) can also alter the intermolecular interactions.[20] Monovalent ions such as Na^+ and Cl^- support strong protein interfacial assembly by promoting the hydrophobic effect and screening the electrostatic interactions between molecules.[21,22] Divalent Ca^{2+} ions are essential for the polymerization of Lam-111 in bulk solution and on lipids, activating the polymerization by binding to the γ short chains of laminins.[20,23]

The initial increase in surface pressure after Lam-111 droplet deposition was rapid for both pH 4 and 7.5, taking almost similar time frames (≈ 15–20 min) (**Figure 2**A). The final surface pressure (after 120 min) was much higher on a subphase with pH 4 compared to pH 7.5, which is attributed to the greater ability of Lam-111 to anchor and aggregate at pH 4 than at neutral pH.[20] When NaCl (molar concentration c = 100 mm) was added to the subphase with pH 4, the surface pressure during the adsorption of Lam-111 increased further. The effect increased when the NaCl ionic strength in the subphase was doubled (NaCl = 200 mm) (Figure 2A). It is expected that laminins become more hydrophobic when electrostatic charges are screened by monovalent ions, which enhances surface activity. It was further observed that the mechanical strength of the Lam-111 spread films was not different when the ionic strength of NaCl was doubled (200 mm) or when $CaCl_2$ (50 mm $CaCl_2$) was introduced in the subphase when

ADVANCED
SCIENCE NEWS
www.advancedsciencenews.com

ADVANCED
FUNCTIONAL
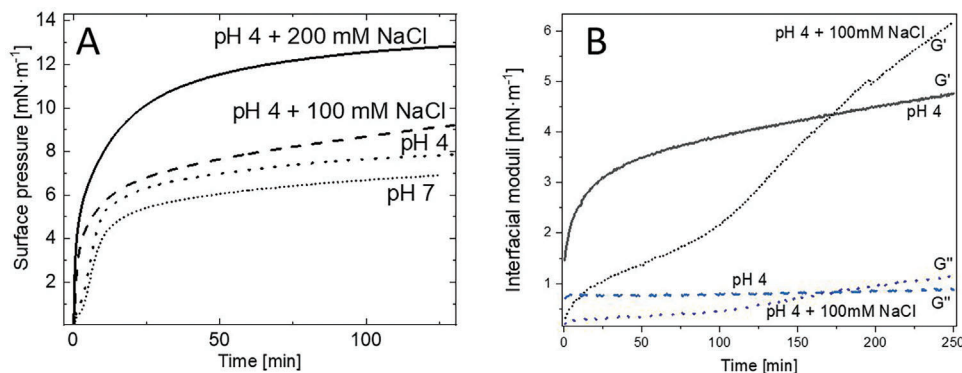**MATERIALS**
www.afm-journal.de

Figure 2. Lam-111 adsorption as a function of pH and Ionic strength: A) Surface pressure and B) interfacial moduli versus time.

compared to the subphase pH 4 with [NaCl] = 100 mM (Figure S2, Supporting Information). These results confirm that Ca^{2+} is not essential for Lam-111 crosslinking at the A–W interface. We propose that while Ca^{2+} ions may initiate the formation of the ternary binding interactions in vivo, they do not actively participate in them and therefore, Ca^{2+} ions do not affect the strength of Lam-111 networks formed under 2D confinement. Hence, for our experiments, the subphase with pH 4 and with [NaCl] = 100 mM was used. The surface pressure suggests that the layer is formed in two stages: a step characterized by a fast increase in surface pressure (15–20 min) and a second step characterized by a gradual increase (several hours). This tendency of Lam-111 is observed independent of subphase pH, ionic strength, amount of Lam-111 spread, or vessel used for layer assembly. We expect that the initial rapid increase step is mainly due to the adsorption of molecules resulting in a condensed layer. The second slow increase step can be attributed to the self-crosslinking of Lam-111, resulting in compaction and insertion of additional molecules.

This hypothesis was verified using nulling-based ellipsometry after depositing Lam-111 films on the subphase pH 4 and with c = 100 mM NaCl (**Figure 3**A). For thin organic films, the ellipsometric angle Δ contains information about both film thickness and refractive index.[24] Recently, we have shown that for Col IV, Δ is proportional to the areal surface excess protein concentration,[25] and we hypothesize that this applies to Lam-111 given its similar structure. As evident in Figure 3A, there

was a fast increase in Δ after spreading and this Δ value plateaus after ≈ 40 min, indicating that the surface excess concentration was relatively constant after this period. A secondary slow increase in Δ shows that there is a possibility of more molecules adsorbing from the subphase at longer time scales. This observation also agrees with the slowly but steadily increasing surface pressure and storage modulus after 40 min. The organization of these monolayers assembled at the A–W interface can provide a better understanding of the structure of laminin layers formed via self-assembly under confinement at the cellular membrane. An important parameter describing the composition of a layer is the packing density. Here, we use the ellipsometry data, previously calibrated for Col IV, which is like Lam-111 a predominantly α-helical protein, making it a reasonable assumption that both have similar optical properties.[25] From the value of Δ after 2 h, we derive an areal concentration of 315 ng cm^{-2} or 3.7×10^{-13} mol cm^{-2}. Then, one laminin molecule covers an area of 450 nm^2. Based on the average short arm length (38 nm) and triangular tiling, the area per molecule would be on the order of 1800 nm^2. Yet, the short arms are flexible and they are also not necessarily parallel to the interface, which enables denser packing. The packing density of proteins at interfaces is usually determined by their concentration in the bulk phase, which might also be valid for the packing density of laminins in the basal lamina.

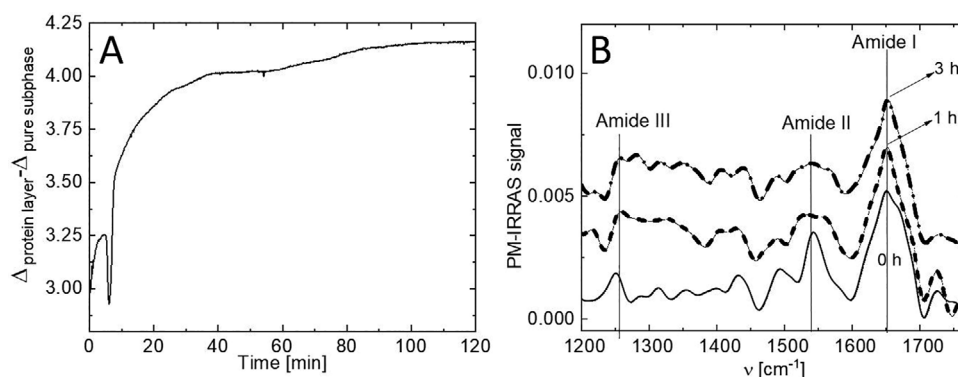The molecular structure of the Lam-111 films during self-assembly at the A–W interface was investigated in situ with

Figure 3. A) Ellipsometric angle Δ and B) PM-IRRAS spectra during adsorption of Lam-111 at the A–W interface of an aqueous subphase with pH 4 and [NaCl] = 100 mM.

**ADVANCED
SCIENCE NEWS**

www.advancedsciencenews.com

**ADVANCED
FUNCTIONAL
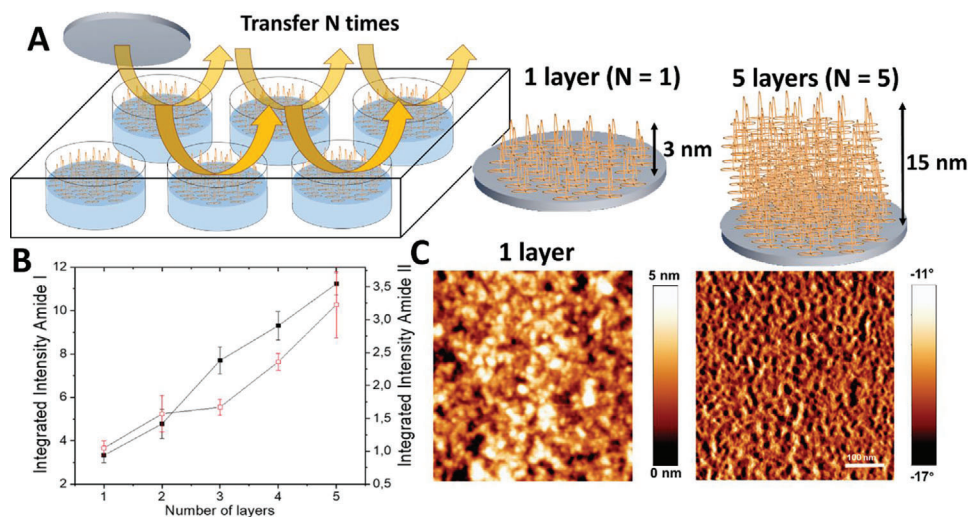MATERIALS**

www.afm-journal.de

Figure 4. A) Schematic representation of the multilayer preparation in a 6-well plate. B) Integrated amide I and amide II intensities of multilayers after each transfer step, measured via PM-IRRAS on a gold-covered glass slide. C) AFM images of a Lam-111 monolayer transferred to a silicon wafer. Left: height. Right: phase.

PM-IRRAS measurements (Figure 3B). The Amide I peak close to 1655 cm^{-1} (C=O stretching of the peptide backbone) is considered to be reliable in predicting the secondary structure of proteins and is typical of α-helical proteins and peptides.[26] Lam-111 exists predominantly as α-helices at the A–W interface (peak position of amide I: 1650 cm^{-1}) (Figure 3B) and no conformational changes occurred during self-assembly. Interestingly, the amide-II peak was much smaller after 1 h. For PM-IRRAS spectra of α-helical proteins at the A–W interface, it has been established that a high ratio of amide I / amide II intensity suggests that the orientation of the helices is close to parallel to the water surface.[27] This is also in line with the layer thickness, which is about twice the diameter of an α-helix.

An important aspect of the structure of the laminin 2D network is the position of the long arms with respect to the network plane. Here, either an upward or downward orientation can be assumed preferentially, or the molecules can be oriented randomly (Figure 1B). The orientation is highly relevant when it comes to molecular recognition and cellular interaction. In vivo, the interaction of the long arms with the cellular membrane and potentially also the short arms with the Col IV layer in the basal lamina can promote a uniform orientation of the long arms toward the epithelium. Whether the polarity gradient at the A–W interface (Figure 1G) can orient the molecules in a similar way is not apparent from the PM-IRRAS spectra. Here, the orientation was determined indirectly by cell-adhesion force measurements (see below).

Interfacial shear rheology was used to prove that Lam-111 is able to crosslink by supramolecular self-assembly at the A–W interface after spreading Lam-111 on different subphases (Figure 2B). The storage modulus (G') of the Lam-111 films increased with time for all subphase conditions. The contribution from the elastic component of the shear modulus was much higher than the contribution of the loss modulus, similar to other proteins that self-assemble at the A–W interface such as lysozyme, and indicates that the layer behaves like a gel and not

like a solution.[21] This confirms that Lam-111 can crosslink at the A–W interface and can explain the secondary slow increase in surface pressure of Lam-111 spread films. For the subphase condition with pH 4, the loss modulus (G'') did not change at all, while for the subphase with pH 4 and c = 100 mm NaCl, there was a linear increase in loss modulus with time for 250 min (Figure 2B). For the former, although the starting elastic modulus was higher than the latter, the value attained after 4 h was lower. Clearly, the presence of salt enhances the mechanical strength of the Lam-111 layer as shown previously for lysozyme.[21] Since Lam-111 forms a quasi-2D network (as visualized in **Figure 4**c), we can derive further information on its structure from the shear modulus. For worm-like chains, $G'_{3D} = c_E * \frac{l_p}{l_E} * k_B T$, where l_p is the persistence length of the chains, l_E is the distance between entanglements and $c_E \approx \frac{1}{l_E^3}$ is the density of entanglements.[28] With $G' \approx 5$ mN/m as in Figure 2B and a thickness d of the network of ≈ 3 nm (see below), we find $G'_{3D} = \frac{G'}{d} = 1.6$ MPa. As the persistence length of laminin is not known, we resort to an estimation that enables us to derive an upper limit for the distance between entanglements. Using the value of $l_p = 160$ nm, which is on the higher end of the range of experimental values for collagen I,[29] we derive an entanglement length of $l_E = 4.5$ nm as an upper limit. Taking into account the molecular dimensions and the areal density derived from ellipsometry, such a short entanglement length suggests that there is a substantial interweaving of the laminin molecules, as the distance between the branch points at the ends of the short arms is more than 30 nm. This is also in line with the AFM phase image of the 2D network, which implies the presence of a high areal density of crossing points.

2.2. Self-Assembled Multilayers and AFM

The self-assembly of laminins in nature is one of the elementary steps required for the formation and maintenance of tissues. Such a process needs to be extremely robust, repeatable, and
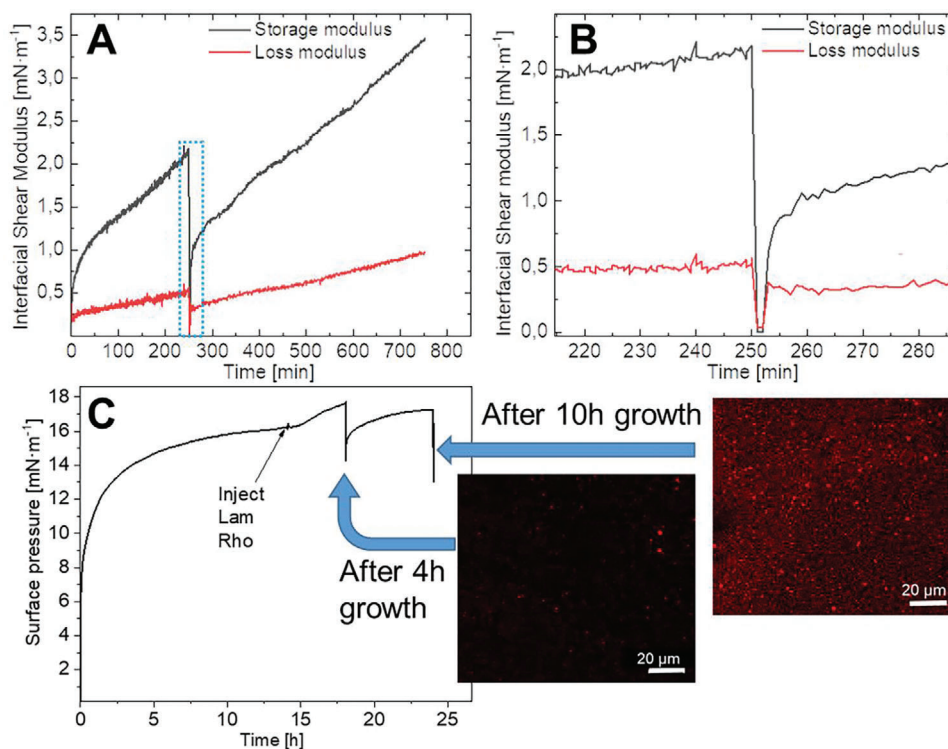
ADVANCED
SCIENCE NEWS

www.advancedsciencenews.com

ADVANCED
FUNCTIONAL
MATERIALS

www.afm-journal.de

Figure 5. Self-healing experiment with Lam-111 layers growing at the A–W interface. At $t = 250$ min, the layer is strained by 500%. B) Magnified view of the region represented by the blue dashed rectangle in A). C) Growth of Lam–111 films till equilibrium surface pressure is reached (14 h), followed by injection of labeled Lam-111 (LamRho) and transfer after further 4 and 10 h. The fluorescence microscopy images correspond to the films transferred after 4 and 10 h of exposure to LamRho.

failure resistant. Here, the knowledge collected from in situ and ex situ characterization of Lam-111 self-assembly in vitro enabled the optimization of the process toward a straightforward and scalable fabrication process for 2D mono- and multilayers using basic lab equipment (Figure 4A).

In a 6-well plate filled with the pH 4 and 100 mM NaCl subphase, the molecules are deposited at the surface and after waiting for self-crosslinking (2 h); the layer can be subsequently transferred by simply touching the substrate held with forceps parallel to the interface in a manual Langmuir–Schäfer transfer. To prove that the amount of protein deposited in each transfer is constant, stacks of 1, 3, and 5 layers were produced on Si-wafers and gold-covered glass slides for characterization by PM-IRRAS (Figure 4B), ellipsometry, and AFM (Figure 4C; Figure S3, Supporting Information). The thickness of a Lam-111 2D network as determined by AFM was 3.2 ± 1 nm. The network-like morphology of the Lam-111 2D networks on the Si-wafer is evident in the AFM phase image (Figure 4C right), while the height image suggests a uniform thin layer (all features below 5 nm in height). For 5 layers, the thickness was fivefold of a single layer at 14.8 ± 2.1 nm (Figure S3, Supporting Information). The thickness was confirmed by ellipsometry measurements, which estimated the thickness of the multilayers to be 8.9 ± 0.1 nm for 3 layers and 16.1 ± 0.3 nm for 5 layers. The thickness of Lam-111 monolayers could not be determined by ellipsometry without knowledge of the layer's refractive index, as the thickness is below the ultra-thin film limit. The precise control over the areal protein concentration was confirmed by PM-IRRAS of Lam-111 films on gold-covered glass performed after each transfer in a multilayer deposition experiment. There was a stepwise linear increase of protein amount (integrated amide I and amide II intensity) with each deposition step (Figure 4B). Conclusively, stacked 2D networks of Lam-111 with defined thickness can be prepared using a multiwell plate, a syringe, and a tweezer.

2.3. Self-Healing, Self-Renewal, and Growth by Dynamic Exchange of Molecules

Due to their inherently delicate nature and permanent exposure to sources of chemical and mechanical damage, 2D materials can only persist when including strong and reliable self-healing mechanisms. A pre-requisite of self-healing is the existence of reversibly forming bonds and the possibility of re-alignment and re-assembly,[30] which is fulfilled by the non-covalent ternary interactions participating in the Lam-111 polymerization. When shearing the polymerized Lam-111 layers after self-crosslinking at 500% strain, the disappearance of the elastic moduli indicates the breaking of the non-permanent bonds (**Figure 5B**). Immediately after shearing, the moduli increase, indicating self-healing of the layer. Interestingly, the time required for the storage modulus to recover to the same value as before the application of the destructive strain (250 min) is almost identical to the time required to reach that initial value (Figure 5A). The thickness and morphology of the layer were unchanged before and after shearing and self-healing (≈8 nm, (Figure S4, Supporting Information)),
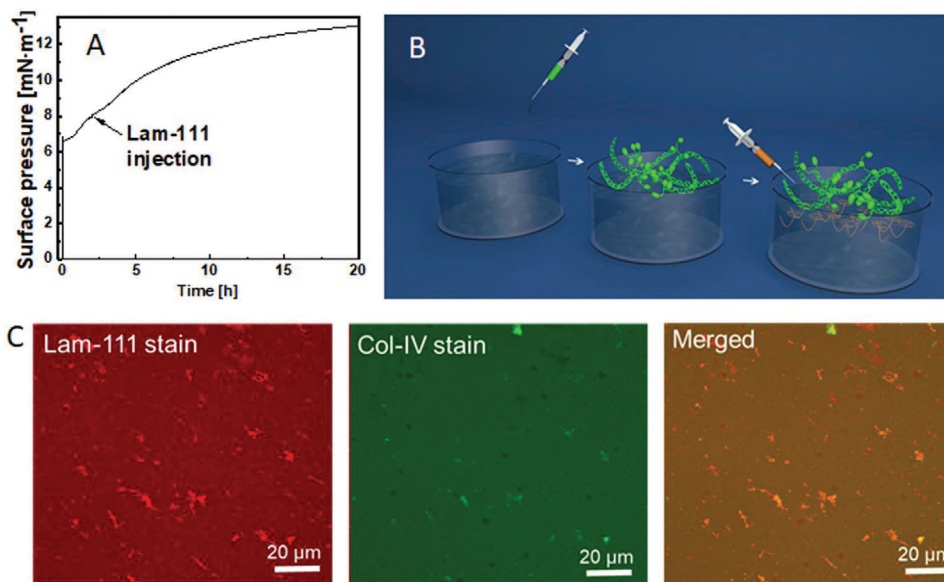
**ADVANCED
SCIENCE NEWS**

www.advancedsciencenews.com

**ADVANCED
FUNCTIONAL
MATERIALS**

www.afm-journal.de

Figure 6. A) Surface pressure during bilayer preparation experiment, where Lam-111 was injected under a preformed Col IV layer B) Schematic representation of bilayer preparation, C) Confocal fluorescence microscopy images after immunofluorescence staining of both components of the Col IV / Lam −111 bilayer.

meaning a contribution of multilayer formation to the recovery of the shear modulus can be ruled out.

The ability of Lam-111 2D networks to undergo self-healing is not surprising given that permanent repairs are required to maintain the integrity of BMs in vivo. Further functions which are essential to the maintenance of healthy tissue are the ability to self-renew and the capability to grow. Clearly, both functions are enabled by dynamic bonds and the exchange of molecules. As long as new molecules are applied to the surrounding solution, the layer is constantly being renewed. Here, this capability is demonstrated by injecting fluorscently labeled LamRho under a preformed Laminin-111 2D network (Figure 5C). While the layer exhibited weak fluorescence when transferred 4 h after injecting LamRho, the layer was uniformly fluorescent when transferred after 10 h. The thickness of the fluorescently labeled Laminin-111 layer (25 ± 4 nm, Figure S5A, Supporting Information) was not greater than the thickness before the injection of LamRho (24.5 ± 5, Figure S5B, Supporting Information), which confirms that the labeling occurred by exchange of molecules, rather than by the growth of adlayers.

The thickness of the material after 14 h of growth was about ten times greater than the thickness after 2 h. The growth of the laminin network at the A–W interface, but also in a basement membrane, is not happening under true 2D confinement, as additional molecules can adsorb from the bulk phase. In analogy to other 2D materials, under such conditions, adlayers form and grow with time. In that sense, the thickness of BMs can be regulated by the amount of laminin secreted by the surrounding cells. Here, an important difference between the situation at the A–W interface and the situation in biological tissues is the ability of the latter to expand. A laminin sheet that is not confined at its periphery can grow laterally. If the sheet is confined at its periphery, it can still increase its area by increasing its curvature, to an extent that leads to folding as, for example, observed in lung tissue.[31]

At the A–W interface, a lateral expansion is possible in a Langmuir trough if the barriers are allowed to open, but the generation of curvature is inhibited by the large surface tension of water (72.8 mN m^{-1} at room temperature), which requires much larger surface pressure than the ≈16 mN m^{-1} generated by Lam-111 (Figure 5C) to overcome. Therefore, here, only growth by adlayer formation is observed.

2.4. (Self-) Assembly at Bio-Interfaces

Based on the robust self-assembly of Lam-111, it is natural to expect that the A–W interface can serve as an in-vitro system to investigate the formation of more complex tissue-like structures. Here, the assembly of laminins on the surface of Col IV sheets, resulting in bilayer structures similar to the basal lamina, is the implied next step. To produce such materials, Col IV was spread at the A–W interface and after 2 h assembly, Lam-111 was injected into the subphase and the layer formation was followed by monitoring the surface pressure (**Figure 6**A). The surface pressure after spreading of Col IV plateaued at ≈8 mN m^{-1} after 2 h, and after injection of Laminin-111, increased to 12 mN m^{-1} within 18 h, at which point the bilayer was transferred to glass substrates by the Langmuir–Schäfer (LS) method. After staining the two different layers, confocal fluorescence microscopy confirmed the growth of a Lam-111 layer on the Col IV layer (Figure 6B). The Lam-111 layer has small aggregations on a film covering the substrate, while the Col IV layer is mostly homogeneous. Since the collagen was not removed from the subphase before injecting the laminin, both could in principle co-adsorb. The fact that the fluorescence from both molecules in Figure 6 barely colocalizes shows that co-adsorption is only of minor importance and that both molecules form mostly separate layers. AFM micrographs of the bilayer (Figure S6, Supporting Information) show a
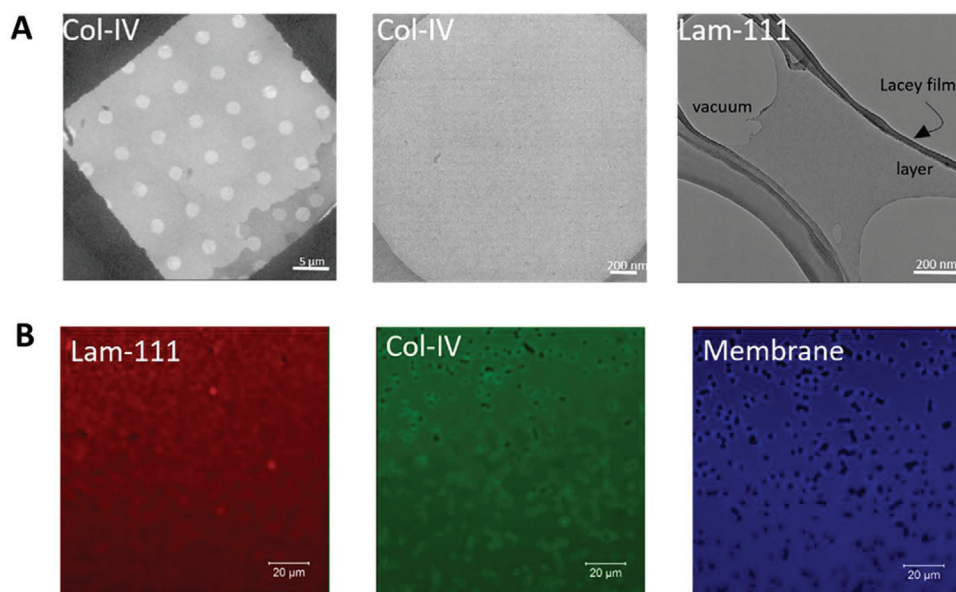
**ADVANCED
SCIENCE NEWS**

www.advancedsciencenews.com

**ADVANCED
FUNCTIONAL
MATERIALS**

www.afm-journal.de

Figure 7. A) TEM of Freestanding Lam-111 monolayer on lacey carbon a film and freestanding Col IV layer on a Quantifoil substrate B) Confocal fluorescence microscopy images after immunofluorescence staining of both components of bilayers on porous Transwell membrane. The picture of the membrane in the blue channel was recorded using the autofluorescence of the membrane material.

similar morphology, appearing as a smooth layer with small aggregations, which corresponds well with the merged confocal microscopy image of the bilayer on glass. The thickness of the bilayer was 22.5 ± 3 nm. This thickness is comparable to the thickness of Col IV networks, meaning that despite the long assembly time, Lam-111 is not forming multilayers when Col IV is covering the interface. These in vitro results support the hypothesis of structural biology that laminins are forming 2D networks by the association of their short arms, which can grow into multilayers and associate with Col IV to form the basal lamina.[11,32]

2.5. Structural Function

The high shear moduli of Lam-111 2D networks imply the possibility of producing freestanding layers. Yet, Lam-111 was only rarely found to survive the transfer to TEM substrates such as lacey carbon (**Figure 7**A). In contrast, Col IV layers repeatedly survived the transfer to TEM substrates with micrometer-sized pores (Figure 7A) when compressed to 20 mN m^{-1}. Based on the finding that Col IV is essential for the mechanical stability of the basal lamina, we developed a two-step procedure to cover porous substrates (Transwell membranes) with a Col IV / Lam-111 bilayer. First, the Col IV layer is transferred onto the porous membrane and then the Lam-111 2D layer is transferred on top of the Col IV layer. Confocal fluorescent microscopy imaging of the immunostained bilayers confirmed that the majority of the pores were covered (Figure 7B). Such samples could, for example, be used for studying the barrier function of the BL in the migration of cancer cells and the transport of drugs. However, studying barrier functions with such thin films requires substantial optimization of the experimental setup and conditions and exceeds the scope of this study.

2.6. Bioinstructivity

It seems plausible that assembling Lam-111 at the Col IV-water interface results in an organization that is closer to the one found in nature than the one produced by successive transfers of the independent monolayers. Clearly, there have to be some cues that direct the construction of the complex tissue architectures found in nature, and the sequence and environment of their assembly must be reflected. To prove this hypothesis, we investigate whether the preparation procedure has an influence on the structure of the material, to an extent that it can be recognized by organisms like cells. Taking into account the different possible orientations of Lam-111 at the A–W interface (long arms on top or bottom of the sheet or no preferential orientation) and the two different possibilities to generate Col IV / Lam-111 bilayers by either step-wise transfer or self-assembly in situ, we arrive at 5 relevant different possibilities to generate and orient the bilayers (see Figure S7, Supporting Information, for fabrication scheme). One can carry out successive transfers and put either laminin or collagen on top. For Laminin, there could be an accumulation of the long-arms on either side of the 2D sheet. Here, Langmuir–Schäfer (LS) transfer exposes the side directed toward the water, while Langmuir–Blodgett (LB) transfer exposes the side directed toward air. In addition, one can expose either the air- or the water side of Col IV using LB and LS transfer, but for a linear molecule oriented parallel to the A–W interface,[25] we expect both sides to be similar and therefore, for Col IV, only carry out LS transfer. Similarly, the orientation of the Lam-111 layers could be varied before covering them with Col IV, but it is unlikely that the orientation of the laminin molecules buried under a relatively thick Col IV layer affects cellular recognition. For all possible combinations, the success of the transfers was confirmed by fluorescence microscopy, using either immunostaining or labeled molecules to confirm the presence of continuous
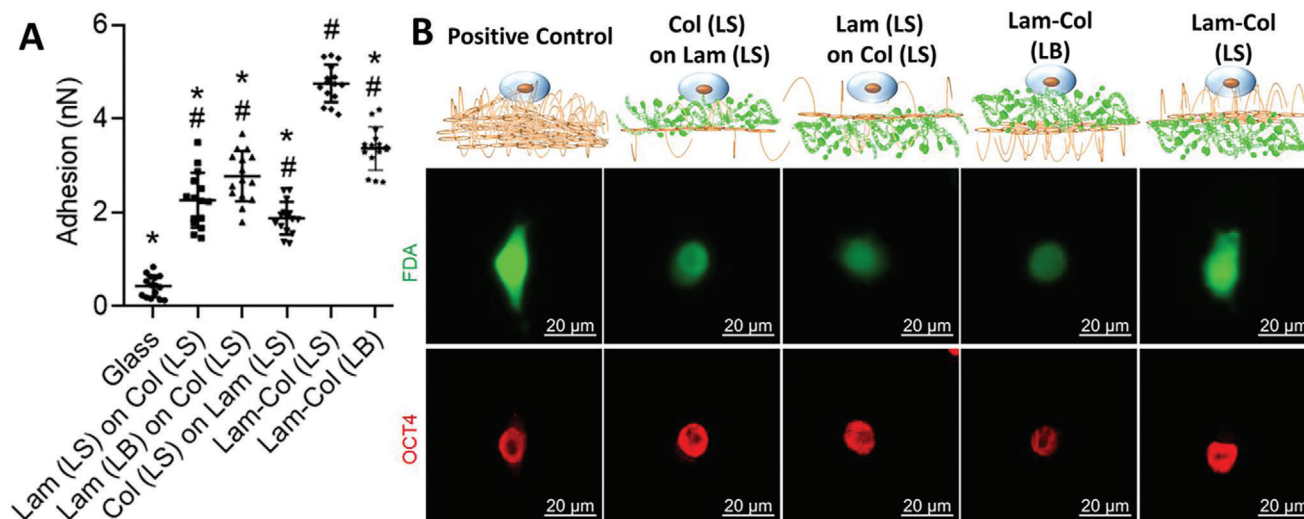
Figure 8. A) miPSCs adhesion onto the 2D Lam-111/Col IV layer. Data are shown as mean SD, and analyzed using one-way ANOVA followed by Tukey's test (# compared to glass, $p < 0.0001$; * compared to Lam-Col (LS), $p < 0.0001$. $n = 15$). B) Top: Schematic representation of the bilayer organization with respect to adhering miPSC. Middle and bottom: Representative fluorescence of miPSC adhered to the 2D Lam/Col layer. Positive control was miPSCs cultured on 10 µg mL^{-1} Lam-111 coated glass. Scale bar = 20 µm.

bilayers (see Figure S8, Supporting Information, for an overview of fluorescence images of mono- and bilayers). Then, the effect of the preparation procedure on the adhesion of induced pluripotent stem cells from mice (miPSC) was investigated. AFM-based single-cell force spectroscopy was used to measure the forces that drive the miPSCs adhesion onto the different 2D protein layers. The cell adhesion onto a certain surface is mediated by the interplay of nonspecific hydrophobic and electrostatic forces as well as specific receptor–ligand recognition.[33] The nonspecific interaction was determined by measuring the adhesion between the cell and a bare glass surface (**Figure 8**A). The nonspecific adhesive force was 0.43 ± 0.23 nN, which was significantly lower when compared to those measured between the cell and the 2D protein layers. Yet, there was a clear difference in the specific adhesion of the miPSC to different Lam-111/Col IV layers, suggesting a difference in the surface density and orientation of recognition sites was discernible for the cells. Considering the observation that the Lam-Col (LS) layer displayed the strongest adhesion affinity for miPSC (4.76 ± 0.40 nN), we deduce that during the self-assembly, the orientation of Lam was precisely arranged by the Col IV layer at the A–W interface. Bilayers produced in that way are capable of replicating the stem-cell niche, as was evidenced by miPSC that could robustly adhere and spread on the Lam-Col (LS) bilayer while maintaining high-level expression of the pluripotency marker OCT4 on a level similar to the positive control (Figure 8B). This confirms that the blueprint for the basal lamina is encoded into the molecular structure of both laminin and Col IV, allowing for the self-assembly of these tissues via molecular recognition, where oriented laminins enable bioinstructivity through selective cell adhesion and spreading. As a result, the self-assembled Lam-Col (LS) bilayer shows great potential for the stable single-cell culture approach, which was introduced to overcome some of the drawbacks of colony passaging.[34] Since Lam (LB) on Col (LS) displays slightly stronger adhesion than Lam (LS) on Col (LS) (Figure 8A),

we infer that the long arms have a slight tendency to gather on the sheet surface directed toward the air also in the absence of Col-IV.

3. Conclusion and Outlook

The complex architectures of natural tissues are encoded in their molecular constituents. Here, we have explored the self-assembly of Lam-111, as the primary cell-instructive component of the basal lamina, into 2D structures similar to those found in nature. We have shown that Lam-111 2D networks, either alone or in combination with Col-IV, display many of the material functions of the basal lamina (**Table 1**). The functions required for tissue maintenance and growth are imparted by dynamic bonds and the exchange of molecules with the surrounding fluid. The thickness of the Lam-111 networks changes via the formation of adlayers upon prolonged growth under semi-confinement. We were able to show that when Laminin-111 sheets are grown in the absence of Col IV, miPSCs exert weaker adhesion force and have a lower tendency to spread on them, with Col IV seemingly

Table 1. Comparison of the material functions of the basal lamina and the mono- and bilayers prepared in this work. The brackets indicate that this function is highly likely based on the observations, but was not proven unequivocally in a designated experiment.

Function of Basal lamina	Lam-111 or Col-IV-Lam
Bioinstructivity	✓
Structural Function	✓
Selective Barrier	(✓)
Self-healing	✓
Self-renewal	✓
Lateral Growth	(✓)

providing elemental cues for the organization of Lam-111. We have shown that combining Col IV and Lam-111 enables the generation of freestanding basal lamina mimicking bilayers that can be used to cover porous membranes. The self-assembly of both components is remarkably robust and the bilayers can be obtained using nothing more than a syringe, a vessel, and a tweezer, and it is implied that the procedure can be applied to experimentally challenging problems such as single-cell passaging or the coating of very soft materials like hydrogels and droplets.

The presented methodology is also an exciting pathway to investigate the complexity and nuances of BM formation in vivo. BMs are exceptional macromolecular constructs conceived by nature to support life as early as embryogenesis. However, this construction fails if the polymerization of laminins is disturbed, and therefore, delving deeper into their assembly is of major importance to understanding how life unfolds from embryos to adults. For example, how are non-polymerizing laminins such as laminin-3A32, laminin−3A11, and laminin−421 integrated with polymerizing laminins such as Lam-111 or laminin−521 in nature and how are the functional properties of the basal lamina impacted? The growth of Col IV and Lam-111 bilayers at the A–W interface is clearly just the very beginning of the journey of the preparation of artificial BLs, which, for instance, also include connector molecules such as perlecan or nidogens. It is plausible that the methods discussed here could be used to understand how these molecules are integrating into ultra-thin basal lamina-like layers. Therefore, we hope that the current work will stimulate further investigations in the field of BL research.

4. Experimental Section

Materials: The substrate materials used were PET Porous Transwell PET membranes (Corning, pore diameter = 3 µm), p-type Si-wafer (IMS, Stuttgart, Germany), a gold-coated glass substrate (Arrandee, Werther, Germany), Quantifoil holey carbon films (R 2/4 Cu 400) and Quantifoil lacy carbon films (Quantifoil Micro Tools GmbH, Brückenäckern, Germany), and glass coverslips (Φ = 12 mm, VWR International GmbH, Darmstadt, Germany). Lam-111 from Engelbreth-Holm-Swarm murine sarcoma basement membrane was procured from Sigma–Aldrich (Taufkirchen, Germany), with 1 mg mL^{-1} stock concentration in Tris-buffered NaCl. Aliquots of this solution were made (100 µL) and stored at −20 °C. Solutions were thawed right before use. Lam-111 labeled with Rhodamine or HiLyte 488 dyes was procured from BIOZOL, Eching, Germany. Before use for spreading experiments, 20 µL of Millipore water was added to each vial of labeled Lam-111 to get a stock solution of 1 mg mL^{-1}. To prepare subphases of defined pH and salt concentrations, HCl solution (37% v/v), NaOH pellets (≥98% purity), NaCl powder (≥98.5% purity), and CaCl$_2$ powder (≥96% purity) were procured from Sigma–Aldrich, Germany.

Lam-111 Assembly as Spread Films at the A–W Interface: Lam-111 films were prepared by spreading the protein from concentrated solutions using a syringe (Hamilton, Darmstadt, Germany) directly on the surface of the aqueous subphase at defined pH and NaCl or CaCl$_2$ concentration at room temperature. The experiments were carried out using either a medium size Langmuir trough (Model 312D) with an area of 243 cm^2 or a circular trough (diameter 9 cm), both from KSV NIMA (Helsinki, Finland). In order to adjust the subphase pH of the sterile Millipore water (pH 5.7), 1 or 0.1 M NaOH or HCl prepared in-house was used. The amount of protein spread was 50 µL of 1 mg mL^{-1} Lam-111 for the circular trough and 200 µL of 1 mg mL^{-1} Lam-111 for the medium trough. The subphase, with pH 4 and c = 100 or 200 mM NaCl or 50 mM CaCl$_2$, was prepared by dissolving the required amount of NaCl or CaCl$_2$ in water and adjusting the pH to 4 by addition of NaOH.

Typically, Lam-111 solution was spread on the subphase, and the surface pressure (was measured with a platinum Wilhelmy plate for up to 12 h. For experiments performed overnight, the subphase level was maintained using a commercially available subphase evaporation compensation tool (KSV-NIMA). The tool monitors the surface level through buoyancy and automatically compensates any evaporated subphase liquid with a peristaltic pump.

Fabrication of Lam-111 Mono- and Multilayers: The Lam-111 spread layers were prepared in a 6-well plate (diameter 34.80 mm) from Corning (Kaiserslautern, Germany). Here, 5 mL subphase (pH 4 and [NaCl] = 100 mM) was added to each well of a 6-well plate, and 10 µL of 1 mg mL^{-1} Lam-111 was spread and after 120 min wait time, a layer was transferred onto a substrate by horizontally touching the Lam-111 layer and lifting (Langmuir–Schäfer transfer). The time of 120 min was chosen because it reliably produces monolayers. The subphase used was pH 4 with [NaCl] = 100 mM . The substrates used for morphology and thickness determination of Lam-111 layers were Si-wafers and for quantification of the protein amount using PM-IRRAS was a gold-covered glass substrate. All the steps were performed at room temperature (25 °C).

Dynamic Growth of Lam-111 Layers at A–W Interface: Lam-111 growth at the A–W interface was investigated in a custom-made Langmuir trough (Kibron, Helsinki, Finland). The setup was modified using specially constructed spacers (Kibron) to reduce the surface area for layer formation, and thereby reduce the amount of starting material to be spread. The trough area was 50 cm^2, and the volume of subphase used was 10 mL of pH 4 and[NaCl] = 100 mM solution.

For the Lam-111 growth experiment, 20 µL of 1 mg mL^{-1} laminin solution was spread on the subphase, and the surface pressure was allowed to stabilize for 14 h, and then 20 µL of 1 mg mL^{-1} Rhodamine-labeled Lam-111 (Hölzel Diagnostika Handels GmbH, Köln, Germany) was injected from the subphase. The layer assembly was followed using surface pressure measurements. The inclusion of labeled molecules was detected by confocal fluorescence microscopy (LSM 780 microscope, Carl Zeiss, Germany) of films on glass coverslips transferred after 4 and 10 h after injection of labeled Lam-111.

For investigating the assembly of Lam-111 on Col IV networks, at first 100 µL of 1 mg mL^{-1} Col IV in acetic acid was assembled for 2 h on pH 4 and [NaCl] = 100 mM solution. Then, 50 µL of 1 mg mL^{-1} of Lam-111 was injected and the surface pressure was recorded for 14 h. The Col-IV solution was not removed or exchanged before injecting the Lam-111 solution.

After LS transfer and immunostaining, the layers were visualized by confocal fluorescence microscopy. The detailed staining protocol can be found in Figure S8 (Supporting Information).

Transfer of Col IV/Lam-111 Layers on TEM-Grids: The Quantifoil holey carbon and lacey carbon TEM-grids were cleaned for 5 min at 10 W using a MiniFlecto plasma cleaner (Gala Instrumente GmbH, Bad Schwalbach, Germany). After LS transfer of 1Lam on Quantifoil, the substrate was fixed with 4% (w/v) paraformaldehyde (Merck, Darmstadt, Germany) diluted in phosphate buffer saline (PBS; Biochrom AG, Berlin, Germany), washed with Milli-Q water and allowed to air-dry at ambient temperature and was used for TEM imaging immediately.

The Col IV transfer onto Quantifoil was performed by LB transfer. In brief, the substrate was kept immersed in the subphase (pH 7.5 + 100 mM NaCl) on a medium area Langmuir trough with a dipping well. Col IV solution (200 µL of 1 mg mL^{-1}) was spread as droplets on 225 mL of subphase. After 30 min equilibration, the barriers were compressed to a target surface pressure of 20 mN m^{-1} and after 5 min, the substrate was moved upward from the subphase at a speed of 3 mm min^{-1}.

Preparation of Bi-Layer Col IV and Lam-111 on Porous Membrane: The porous PET membrane (Corning, pore diameter = 3 µm) was cut from the Transwell with a scalpel. At first, Col IV was transferred onto the membrane by the LB method as described above. Thereafter, a second layer of Lam-111 was transferred via LS transfer of 1Lam onto the membrane.

Preparation of Col IV and Lam-111 Bi-Layers on Glass Substrates for Cell Adhesion: The Lam-111 spread layers were prepared in a 6-well plate (diameter 34.80 mm) from Corning (Kaiserslautern, Germany). Here, 5 mL subphase (pH 4 with c = 100 mм NaCl) was added to each well of a 6-well plate and 10 µL of 1 mg mL^{-1}. Col IV layers were assembled by spreading 100 µL of 1 mg mL^{-1} Col IV in acetic acid and left for 2 h on the subphase (pH 4 and [NaCl] = 100 mM) before transfer. Glass coverslips were cleaned with ethanol and dried before transfer. For the assembly of Lam-111 on Col IV, at first 100 µL of 1 mg mL^{-1} Col IV in acetic acid was spread and assembled for 2 h on the subphase (pH 4 and [NaCl] = 100 mм . Thereafter, 50 µL of 1 mg mL^{-1} of Lam-111 was injected into the subphase, and layer formation was permitted for 14 h. The Col-IV solution was not removed or exchanged before injecting the Lam-111 solution.

For LS transfer, the layer was simply taken off by touching with the (precoated) substrate oriented parallel to the interface. For LB transfer of the bilayer onto an empty substrate, to avoid a double coating, two substrates were put face to face and dipped into the well close to the wall. Then, one of the substrates was allowed to slide down, and the other one was moved along the wall to the other side of the well and withdrawn slowly. For LB transfer of Lam-111 onto the precoated substrate, the precoated substrate was immersed in the well before Lam-111 was spread and withdrawn slowly with a dipper at a tilt angle of ≈45° once the layer had formed. For all procedures, the capability of transferring cohesive Lam-111 and Col IV layers was confirmed by fluorescence microscopy using either immunostaining or labeled molecules.

Interfacial Rheology: A rotational rheometer (MCR502, Anton Paar GmbH, Graz, Austria) with biconical bob geometry was used. The setup consists of the biconical bob disk, which can be rotated or oscillated and is connected to a motor, which can detect torque τ, displacement, and rotational angle γ, while the sample is held stationary in a measuring cell. The circular measuring cell consists of a cup fixed to the bottom part of the rheometer with a flange (cup inner radius R_1 = 40 mm, cup height h = 45.00 mm, disk radius R_2 = 34.14 mm, cone angle α = 5°). The entire cell was covered by an insulation jacket to minimize evaporation of fluids. The measuring position of the biconical disk at the interface was detected using a normal force sensor and the system can be easily aligned to ensure reproducible measurements. After the cell was filled with a subphase volume of 35 mL, the biconical bob was positioned at the interface and 50 µL of 1 mg mL^{-1}) Lam-111 was spread at the edge of the vessel. The shear stress is calculated from the measured torque using the formula:

$$\tau_{sh} = g_f \, \tau, \quad g_f = \frac{1}{4\pi}\left(\frac{1}{R_1^2} - \frac{1}{R_2^2}\right) \tag{1}$$

Where g_f is a geometrical factor.[35] Equation (1) is applicable to surface layers of arbitrary viscoelastic behavior in the case of a narrow gap, that is, for R_2-R_1/R_1 ≤ 0.1.

For the oscillatory experiments, the rotational angle was oscillated with a fixed amplitude γ_a and frequency ν. Maximum shear stress of γ_a = 0.3% and a frequency of ν = 0.1 Hz were used. These parameters assured that the layer was within the linear viscoelastic regime as determined by amplitude sweeps. In an oscillatory regime, the variations of the rotational angle are sinusoidal and can be expressed as:

$$\gamma = \gamma_a \, \sin \omega t \tag{2}$$

$\omega = 2\pi\nu$ is the angular frequency.

The measured shear stress can be expressed with respect to G' storage and G'' loss modulus as follows:

$$\frac{\tau_{sh}}{\gamma_a} = G' \sin \omega t + G'' \cos \omega t \tag{3}$$

The interfacial shear and loss moduli G', G'', and the interfacial shear viscosity were calculated using the algorithm provided with the rheocompass software package. The mathematical treatment of the biconical bob rheometer applied used here was described elsewhere.[36]

Self-Healing of Lam Layers at A–W Interface: For the self-healing experiments, the Lam-111 layer was allowed to self-crosslink for 4 h. These experiments were performed using the same interfacial rheology setup as described above. After the crosslinking period of 4 h, the layer was sheared at 500% strain for 2 min and self-healing was followed for 500 min. A strain of 0.3% and a deformation frequency of 0.1 Hz were used for the shear measurements during cross-linking and self-healing phases. The sheared Lam-111 layer and the layer after self-healing of Lam-111 for 500 min were transferred onto Si-wafers, and the layers were characterized for morphology and thickness using AFM.

Ellipsometry: Ellipsometry was performed using an imaging ellipsometer (nanofilm_ep3, Accurion, Göttingen, Germany) with a 658 nm class IIIB laser source in combination with a 10X magnification lens and a CCD camera (768 × 572 pixels). These experiments were executed on the spread Lam-111 layers on the subphase pH 4 with c = 100 mм NaCl in the circular trough. Continuous measurements of the ellipsometric angle Δ were carried out after Lam-111 was spread on the subphase. Here, a constant angle of incidence of 50° and a laser of wavelength 658 nm were used.

For the determination of the thickness of the Lam-111 multilayers on a Si-wafer, ellipsometry was performed to obtain absolute values of Δ and ψ, and one zone was analyzed. The evaluation of the results was performed with the nanofilm_ep4model software (Accurion, Göttingen, Germany). For the determination of the thickness and refractive index, a four-layer model Si-SiO₂-Lam-111-air was used, where the refractive index and thickness of the Lam-111 layers were used as variables. Since the optical properties of air, Si and SiO₂, and water are known, the required parameters of the Lam-111 layer can be derived.

PM-IRRAS: PM-IRRAS allows for surface-specific acquisition of FT-IR spectra of materials because of the differences in the reflection of p- and s-polarized light from interfaces. Spectra were measured using the PMI-550 device from Biolin Scientific mounted on top of a Langmuir trough (Area = 243 cm²). It contains a photo-elastic modulator from Hinds Instruments that modulates the polarization of the light. The normalized differential reflectivity spectrum S is calculated from the collected difference (ΔR) and sum spectra (ΣR) of the detected intensities of the p- and s-polarized light as

$$s = \frac{\Delta R}{\sum R} = \frac{(R_S - R_P)}{(R_S + R_P)} \tag{4}$$

The frequency of the photo-elastic modulator was adjusted to achieve maxima in the region around 1500 cm^{-1}, where the most interesting protein bands of Amide I (1550) and Amide II (1660) are located.

Lam-111 assembly at the A–W interface was followed by measuring the PM-IRRAS spectra at intervals of 0, 1, and 2 h after spreading the Lam-111 molecules at the A–W interface. The spectra were measured for 500 s for each time point and normalized to the spectra of pure subphase (background spectra).

For the substrates coated with Lam-111 multilayers, the spectra were measured for 300 s and the bare gold substrate was used for background correction. The measurements were made after each LS transfer with a drying step in between, and the integrated amide I and amide II intensities are plotted against the number of layers.

AFM of 2D Lam-111 Networks and TEM of Freestanding Layers of Lam-111 and Col IV: AFM was carried out with a Nanowizard4 (JPK, Colditzstraße, Germany) in alternating contact mode using a cantilever OMCL-AC200TS-R3 (OLYMPUS, Tokyo, Japan) of spring constant 9 N/m in air to acquire topography and phase images of the Si-wafer coated with 1Lam.

Transition electron microscopy (TEM) investigations were performed on a Talos F200A (FEI, Eindhoven, The Netherlands) with a high-brightness electron source (X-FEG) and an information limit of 0.12 nm. The prepared samples were all analyzed at 200 kV using a CompuStage Single-Tilt holder (FEI, Eindhoven, Netherlands). The images were obtained with a CMOS technology-based camera model Ceta 16 м (FEI, Eindhoven, the Netherlands) with 4000 × 4000 pixels.

Cell Maintenance: The murine induced pluripotent stem cells (miPSCs, APS0004) were purchased from Riken, Japan. The cells were cultured

in the ESGRO Complete Medium (Merck Millipore, Germany). miPSCs were dissociated into single cells using the ESGRO Complete Accutase (Merck Millipore, Germany). The single cells could be used for cell expansion or further measurements.

Immunofluorescence Staining of miPSCs: miPSCs were fixed with 4% w/v paraformaldehyde and permeabilized with 0.2% v/v Triton X-100 48 h after seeding. Antibodies against OCT4 were used to evaluate the pluripotency, and fluorescein diacetate (FDA, F1303, ThermoFisher, Germany) was used to assess the cell viability. Confocal fluorescence imaging was carried out using an LSM 780 microscope (Carl Zeiss, Germany).

Measurement of the Cell-Substrate Adhesion through AFM: The measurements were performed in the ESGRO Complete Medium supplied with 25 mM HEPES (ThermoFisher, Germany) at 37 ± 0.1 °C controlled by a JPK-AFM system with the CellHesion module (JPK Instruments, Germany). A tip-less cantilever (TL-CONT, NanoSensors GmbH, Germany) was coated with 1 mg mL^{-1} mouse Laminin (Sigma–Aldrich, Germany) at 37 °C for 1 h before the measurement. The actual spring constant of the cantilever was measured based on the thermal noise method. A single miPSC was captured by the Laminin-coated cantilever and then brought in contact with the target surface until a preset contact force of 2.0 nN was reached. The cell remained in contact with the target surface for 5 s. Next, the cantilever was retracted 70 μm away from the target surface to achieve complete separation between the cell and the surface. The piezo movement, as well as the deflection of the cantilever, were recorded via JPK SPMControl software. Force curves were acquired, and the adhesion was calculated using JPKSM Data Processing software (JPK, Germany).

Statistics and Error Considerations: All Lam-111 spreading experiments were performed at least three times on the different subphase conditions. The reported surface pressure curves and interfacial rheology curves are the average curves from the independent experiments. The maximum deviation between the individual measurement curves and the average curves was 6% for surface pressure measurements and 14% for interfacial rheology throughout the experiment. Statistical differences for the mean values of cell-substrate adhesion through AFM were determined using one-way ANOVA followed by Tukey's test, # or * indicate statistically significant differences for $p < 0.0001$ when compared to glass or Lam-Col (LS), respectively.

Supporting Information

Supporting Information is available from the Wiley Online Library or from the author.

Conflict of Interest

The others intend to submit a patent application that is in part based on the presented scientific results and experimental procedures.

Author Contributions

T.B. and Y.N. contributed equally to this work. T.B. performed conceptualization, methodology, investigation, visualization, and writing the original draft. Y.N. performed methodology, investigation, visualization, and writing the original draft. R.M. performed conceptualization, methodology, investigation, project administration, supervision, visualization, and writing the original draft. N.M. performed conceptualization, methodology, supervision, project administration, and writing the review and editing. A.L. performed conceptualization, methodology, supervision, project administration, and writing the review and editing.

[1] W. Wang, A. D. Schlüter, *Macromol. Rapid Commun.* **2019**, *40*, 1800719.

[2] R. Mas-Ballesté, C. Gómez-Navarro, J. Gómez-Herrero, F. Zamora, *Nanoscale* **2011**, *3*, 20.

[3] a) Z. Zhang, X. Liu, J. Yu, Y. Hang, Y. Li, Y. Guo, Y. Xu, X. Sun, J. Zhou, W. Guo, *Wiley Interdiscip. Rev. Comput. Mol. Sci.* **2016**, *6*, 324; b) V. K. Sangwan, M. C. Hersam, *Ann. Rev. Phys. Chem.* **2018**, *69*, 299; c) D. Akinwande, C. J. Brennan, J. S. Bunch, P. Egberts, J. R. Felts, H. Gao, R. Huang, J.-S. Kim, T. Li, Y. Li, K. M. Liechti, N. Lu, H. S. Park, E. J. Reed, P. Wang, B. I. Yakobson, T. Zhang, Y.-W. Zhang, Y. Zhou, Y. Zhu, *Extreme Mech. Lett.* **2017**, *13*, 42.

[4] C. W. Harland, M. J. Bradley, R. Parthasarathy, *Proc. Natl. Acad. Sci. U. S. A.* **2010**, *107*, 19146.

[5] L. Cademartiri, K. J. M. Bishop, *Nat. Mater.* **2015**, *14*, 2.

[6] a) J. Mantaj, T. Abu-Shams, Z. Enlo-Scott, M. Swedrowska, D. Vllasaliu, *Mol. Pharmaceutics* **2018**, *15*, 5802; b) R. Jayadev, D. R. Sherwood, *Curr. Biol.* **2017**, *27*, R207.

[7] D. A. C. Walma, K. M. Yamada, *Development* **2020**, *147*, dev175596.

[8] J. K. Mouw, G. Ou, V. M. Weaver, *Nat. Rev. Mol. Cell Biol.* **2014**, *15*, 771.

[9] C. Leclech, C. F. Natale, A. I. Barakat, *J. Cell Sci.* **2020**, *133*.

[10] N. Khalilgharibi, Y. Mao, *Open Biol.* **2021**, *11*, 200360.

[11] E. Hohenester, P. D. Yurchenco, *Cell Adhes. Migr.* **2013**, *7*, 56.

[12] A. Domogatskaya, S. Rodin, K. Tryggvason, *Ann. Rev. Cell Dev. Biol.* **2012**, *28*, 523.

[13] J. Xu, D. Mosher, in *The Extracellular Matrix: an Overview* (Ed.: R. P. Mecham), Springer Berlin, Heidelberg **2011**, 41.

[14] M. Durbeej, *Cell Tissue Res.* **2010**, *339*, 259.

[15] a) R. Nishiuchi, J. Takagi, M. Hayashi, H. Ido, Y. Yagi, N. Sanzen, T. Tsuji, M. Yamada, K. Sekiguchi, *Matrix Biol.* **2006**, *25*, 189; b) L. Hagbard, K. Cameron, P. August, C. Penton, M. Parmar, D. C. Hay, T. Kallur, *Philos. Trans. R. Soc., B* **2018**, *373*; c) W.-M. Yu, Z.-L. Chen, A. J. North, S. Strickland, *J. Cell Sci.* **2009**, *122*, 929.

[16] A. Purvis, E. Hohenester, *J. Biol. Chem.* **2012**, *287*, 44270.

[17] Z. Xiang, D. Cao, L. Dai, *Polym. Chem.* **2015**, *6*, 1896.

[18] G. W. Laurie, J. T. Bing, H. K. Kleinman, J. R. Hassell, M. Aumailley, G. R. Martin, R. J. Feldmann, *J. Mol. Biol.* **1986**, *189*, 205.

[19] O. Gafni, L. Weinberger, A. A. Mansour, Y. S. Manor, E. Chomsky, D. Ben-Yosef, Y. Kalma, S. Viukov, I. Maza, A. Zviran, Y. Rais, Z. Shipony, Z. Mukamel, V. Krupalnik, M. Zerbib, S. Geula, I. Caspi, D. Schneir, T. Shwartz, S. Gilad, D. Amann-Zalcenstein, S. Benjamin, I. Amit, A. Tanay, R. Massarwa, N. Novershtern, J. H. Hanna, *Nature* **2013**, *504*, 282.

[20] E. Freire, T. Coelho-Sampaio, *J. Biol. Chem.* **2000**, *275*, 817.

[21] A. S. Malcolm, A. F. Dexter, A. P. Middelberg, *Langmuir* **2006**, *22*, 8897.

[22] a) S. A. Roberts, I. W. Kellaway, K. M. G. Taylor, B. Warburton, K. Peters, *Langmuir* **2005**, *21*, 7342; b) A. M. Hyde, S. L. Zultanski, J.

**ADVANCED
SCIENCE NEWS**

www.advancedsciencenews.com

**ADVANCED
FUNCTIONAL
MATERIALS**

www.afm-journal.de

H. Waldman, Y.-L. Zhong, M. Shevlin, F. Peng, *Org. Process Res. Dev.* **2017**, *21*, 1355.

[23] K. Onuma, N. Kanzaki, *J. Phys. Chem. B* **2003**, *107*, 11799.

[24] a) M. F. Mora, J. L. Wehmeyer, R. Synowicki, C. Garcia, in *Investigating Protein Adsorption via Spectroscopic Ellipsometry*, Springer, New York, NY **2009**; b) H. Motschmann, R. Teppner, in *Ellipsometry in Interface Science*, Elsevier, Amsterdam, Netherlands **2001**.

[25] T. Bhuvanesh, R. Machatschek, L. Lysyakova, K. Kratz, B. Schulz, N. Ma, A. Lendlein, *Biomed. Mater.* **2019**, *14*, 024101.

[26] A. Barth, *Bioch. Biophys. Acta* **2007**, *1767*, 1073.

[27] I. Cornut, B. Desbat, J. M. Turlet, J. Dufourcq, *Biophys. J.* **1996**, *70*, 305.

[28] K. Kroy, E. Frey, *Phys. Rev. Lett.* **1996**, *77*, 306.

[29] N. Rezaei, A. Lyons, N. R. Forde, *Biophys. J.* **2018**, *115*, 1457.

[30] M. He, X. Chen, D. Liu, D. Wei, *Chin. Chem. Lett.* **2019**, *30*, 961.

[31] L. Knudsen, M. Ochs, *Histochem. Cell Biol.* **2018**, *150*, 661.

[32] W. Halfter, P. Oertle, C. A. Monnier, L. Camenzind, M. Reyes-Lua, H. Hu, J. Candiello, A. Labilloy, M. Balasubramani, P. B. Henrich, M. Plodinec, *FEBS J.* **2015**, *282*, 4466.

[33] a) L. Sirghi, J. Ponti, F. Broggi, F. Rossi, *Eur. Biophys. J.* **2008**, *37*, 935; b) A. V. Taubenberger, D. W. Hutmacher, D. J. Muller, *Tissue Eng., Part B* **2014**, *20*, 40.

[34] E. Cruvinel, I. Ogusuku, R. Cerioni, S. Rodrigues, J. Gonçalves, M. E. Góes, J. M. Alvim, A. C. Silva, V. d. S. Lino, E. Boccardo, E. Goulart, A. Pereira, R. Dariolli, M. Valadares, D. Biagi, *SAGE Open Med.* **2020**, *8*, 205031212096645.

[35] K. D. Danov, P. A. Kralchevsky, G. M. Radulova, E. S. Basheva, S. D. Stoyanov, E. G. Pelan, *Adv. Colloid Interface Sci.* **2015**, *222*, 148.

[36] P. Erni, P. Fischer, E. J. Windhab, V. Kusnezov, H. Stettin, J. Läuger, *Rev. Sci. Instrum.* **2003**, *74*, 4916.

2304268 (13 of 13)